

## Supplementary Data

### The Three-Dimensional Structural Basis of Type II Hyperprolinemia

Dhiraj Srivastava<sup>1</sup>, Ranjan K. Singh<sup>1</sup>, Michael A. Moxley<sup>2</sup>, Michael T. Henzl<sup>3</sup>, Donald F. Becker<sup>2</sup>, and John J. Tanner<sup>1,3,\*</sup>

<sup>1</sup>Department of Chemistry, University of Missouri-Columbia, Columbia, MO 65211, USA

<sup>2</sup>Department of Biochemistry, University of Nebraska-Lincoln, Lincoln, NE 68588, USA

<sup>3</sup>Department of Biochemistry, University of Missouri-Columbia, Columbia, MO 65211, USA

\*Corresponding author: Department of Chemistry, University of Missouri-Columbia, Columbia, MO 65211, USA; email: [tannerjj@missouri.edu](mailto:tannerjj@missouri.edu); phone: 573-884-1280; fax: 573-882-2754

## **Table of Contents**

<b>Table S1.</b> Kinetic constants for HsP5CDH.	S-3
<b>Figure S1.</b> Superposition of HsP5CDH and MmP5CDH.	S-4
<b>Figure S2.</b> Electron density for the active site of the MmP5CDH-sulfate complex.	S-5
<b>Figure S3.</b> Electron density for the catalytic loops of HsP5CDH and S352A.	S-6
<b>Figure S4.</b> Mutation of Ser352 to Leu abolishes catalytic activity.	S-7
<b>Figure S5.</b> Lineweaver-Burk plot of HsP5CDH initial velocity and kinetic scheme.	S-8
<b>Figure S6.</b> Global fitting analysis of HsP5CDH kinetics.	S-9
<b>Figure S7.</b> Superposition of HsP5CDH with bacterial P5CDHs.	S-10
<b>Figure S8.</b> A model of OH-GSA bound to MmP5CDH.	S-11
<b>Supplementary References</b>	S-12

**Table S1.** Kinetic constants for HsP5CDH determined from global fitting

Parameter	Best fit value	Lower Bound	Upper Bound
$k_1$ ( $k_{\text{cat}}/K_m$ , NAD)	98.7 mM <sup>-1</sup> s <sup>-1</sup>	74.7 mM <sup>-1</sup> s <sup>-1</sup>	144 mM <sup>-1</sup> s <sup>-1</sup>
$k_{-1}$	0.473 s <sup>-1</sup>	0.294 s <sup>-1</sup>	0.813 s <sup>-1</sup>
$k_2$ ( $k_{\text{cat}}/K_m$ , P5C)	316 mM <sup>-1</sup> s <sup>-1</sup>	253 mM <sup>-1</sup> s <sup>-1</sup>	406 mM <sup>-1</sup> s <sup>-1</sup>
$k_{-2}$ <sup>a</sup>	≤ 300 s <sup>-1</sup>	-	-
$k_3$ <sup>b</sup>	≥ 500 s <sup>-1</sup>	-	-
$k_{-3}$ <sup>c</sup>	0	-	-
$k_4$ <sup>b</sup>	≥ 500 s <sup>-1</sup>	-	-
$k_{-4}$ <sup>d</sup>	0	-	-
$k_5$ ( $k_{\text{cat}}$ )	10 s <sup>-1</sup>	9.1 s <sup>-1</sup>	11 s <sup>-1</sup>
$k_{-5}$ <sup>e</sup>	0	-	-
$k_6$ <sup>f</sup>	81.7 mM <sup>-1</sup> s <sup>-1</sup>	-	-
$k_{-6}$	9.2 s <sup>-1</sup>	5.1	14.8
$K_1 = k_{-6}/k_6$	112 μM	49 <sup>g</sup>	181

<sup>a</sup> $k_{-2}$  has little effect on the initial velocity progress curves and was held fixed to a value of 22 s<sup>-1</sup> but could be ≤ 300 s<sup>-1</sup>.

<sup>b</sup> $k_3$  and  $k_4$  have little effect on the initial velocity progress curves beyond 500 s<sup>-1</sup> and were fixed at 3290 s<sup>-1</sup> and 569s<sup>-1</sup> so that these steps were non rate limiting according to the Theorell-Chance mechanism.<sup>1</sup>

<sup>c</sup> $k_{-3}$  was fixed to zero based on the previous observation of no observable turnover in the reverse direction.

<sup>d</sup> $k_{-4}$  was fixed to zero according to the Theorell-Chance mechanism.

<sup>e</sup> $k_{-5}$  was fixed to zero based on the observation of a  $K_d \geq 1$  mM (data not shown). Once  $k_{-5}$  is 10-fold below  $k_5$  it has no effect on the progress curves.

<sup>f</sup> $k_6$  was held fixed to obtain an error on the  $K_1$ ; this step is at equilibrium and thus the fixed rate constant shown here is only the best fit value and should not be considered as a constrained estimate of this rate constant.

<sup>g</sup>The percent error from the bounds of  $k_{-6}$  was used to estimate a rigorous boundary for the  $K_1$ .

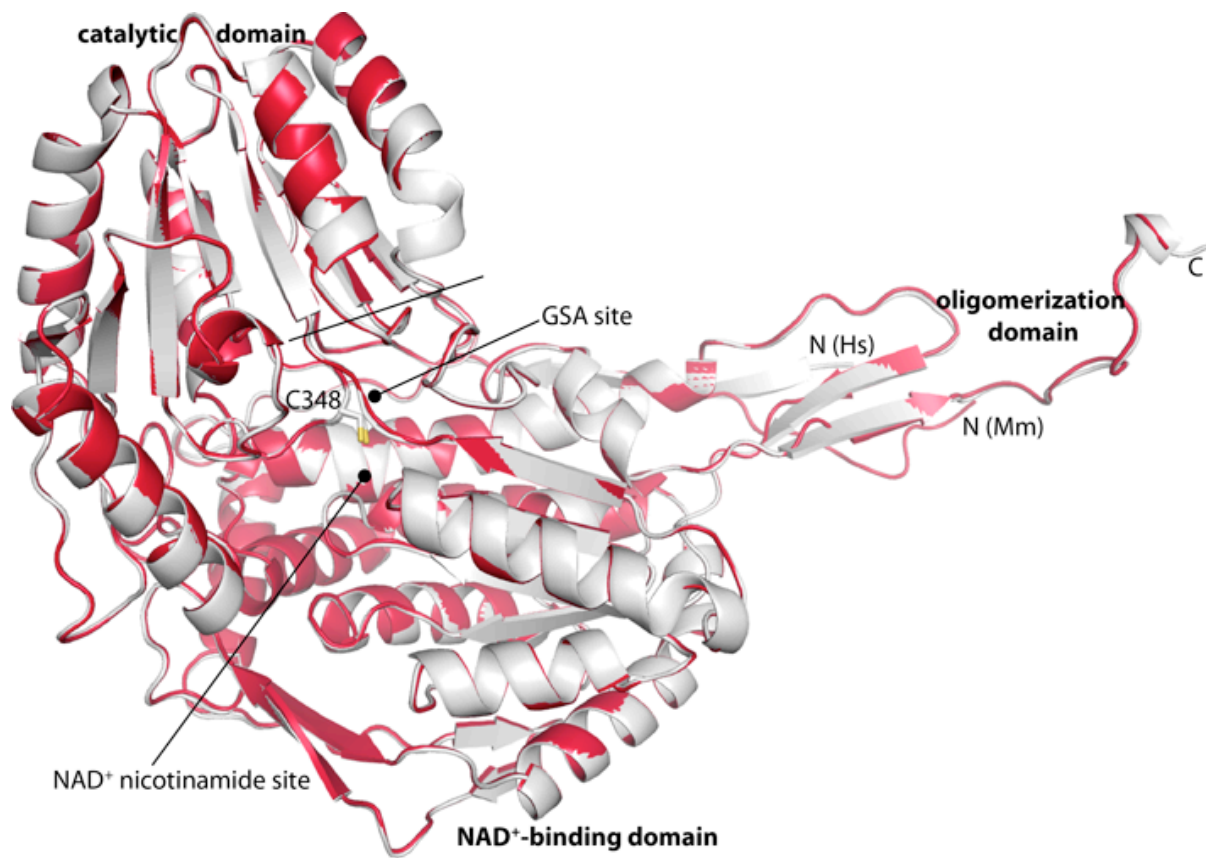


**Figure S1.** Superposition of HsP5CDH (white) and MmP5CDH (red).

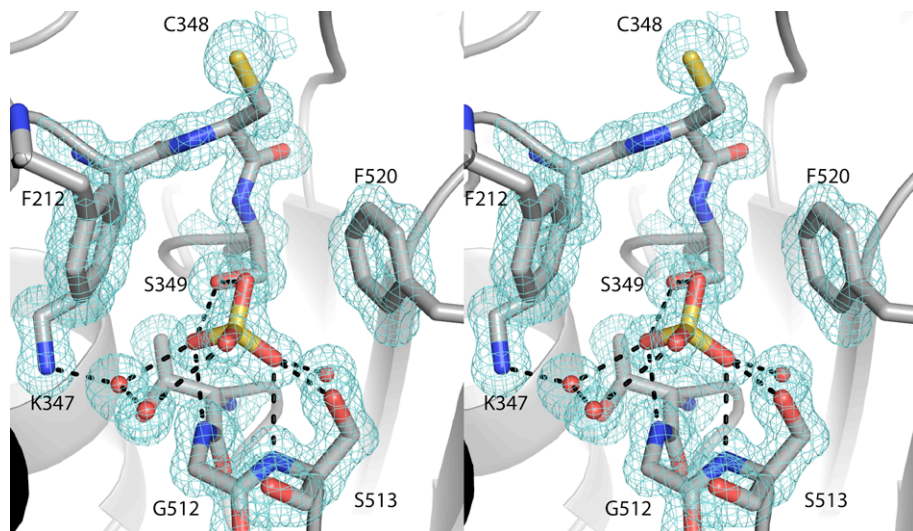


**Figure S2.** Electron density for the active site of the MmP5CDH-sulfate complex (stereographic view). The cage represents a simulated annealing  $\sigma_A$ -weighted  $F_o - F_c$  omit map contoured at  $3.0 \sigma$ .

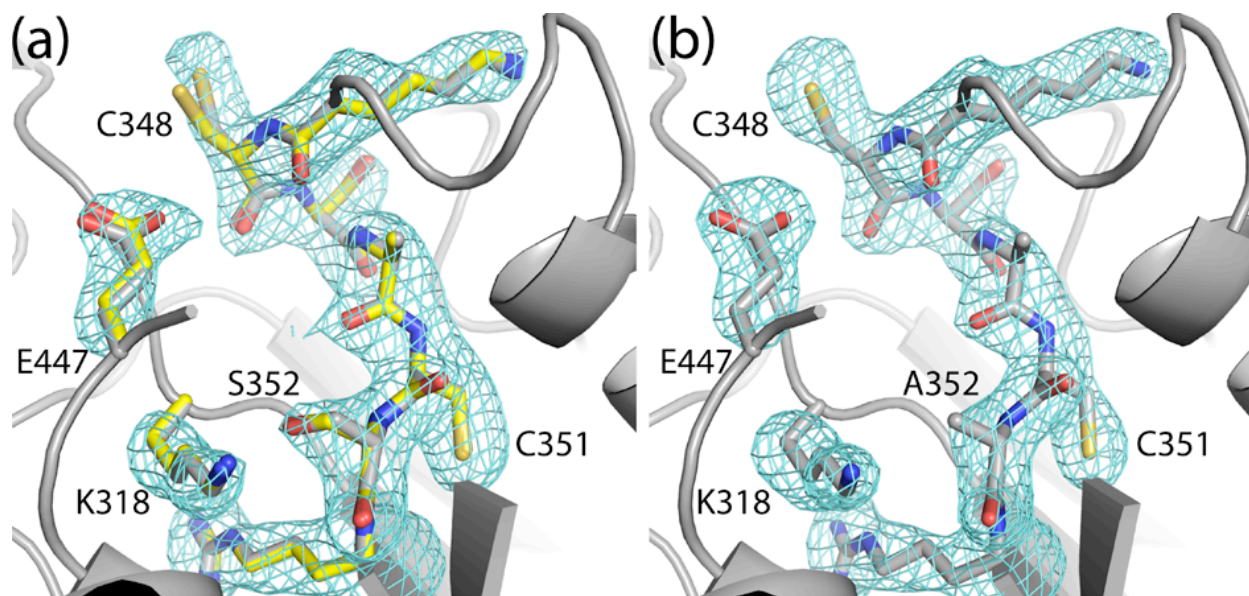


**Figure S3.** Electron density for the catalytic loops of (a) HsP5CDH and (b) S352A. (a) Superposition of HsP5CDH (gray) and MmP5CDH (yellow). The cage represents a simulated annealing  $\sigma_A$ -weighted  $F_o - F_c$  omit map for HsP5CDH contoured at  $3.0 \sigma$ . Note that the two enzymes have almost identical active site conformations. (b) Catalytic loop of S352A shown in the same orientation as in panel a. The cage represents a simulated annealing  $\sigma_A$ -weighted  $F_o - F_c$  omit map contoured at  $3.0 \sigma$ . Note that the conformation of the active site of S352A is nearly identical to those of HsP5CDH and MmP5CDH.

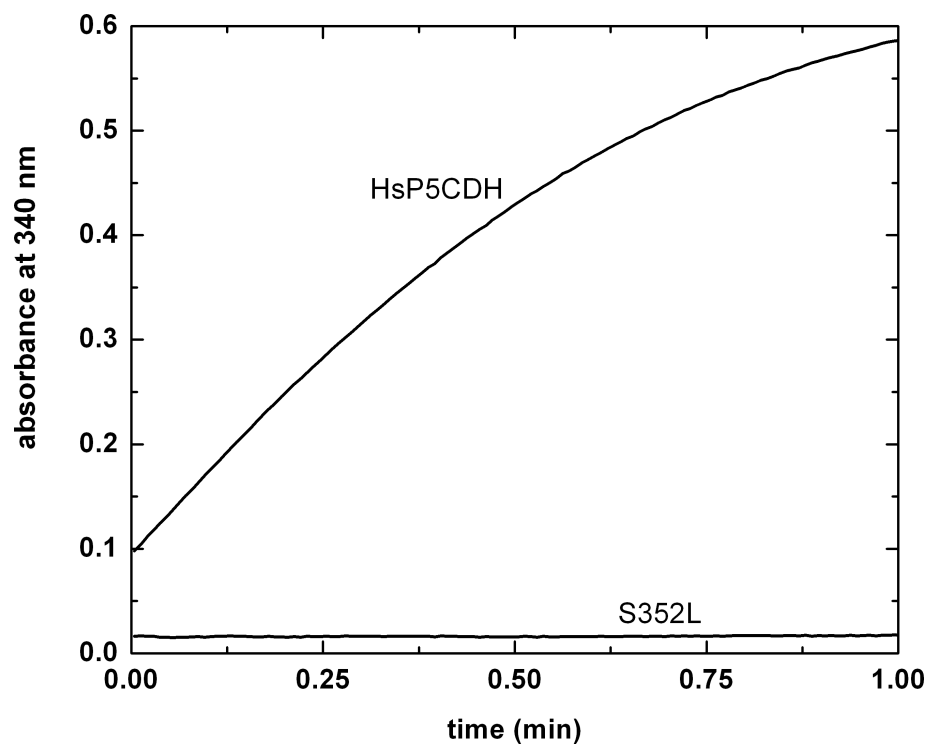


**Figure S4.** Mutation of Ser352 to Leu abolishes catalytic activity. Progress curves for HsP5CDH and S352L. The  $\text{NAD}^+$  and P5C concentrations are  $350 \mu\text{M}$  and  $200 \mu\text{M}$ , respectively. The concentration of S352L is 10-fold higher than that of HsP5CDH.

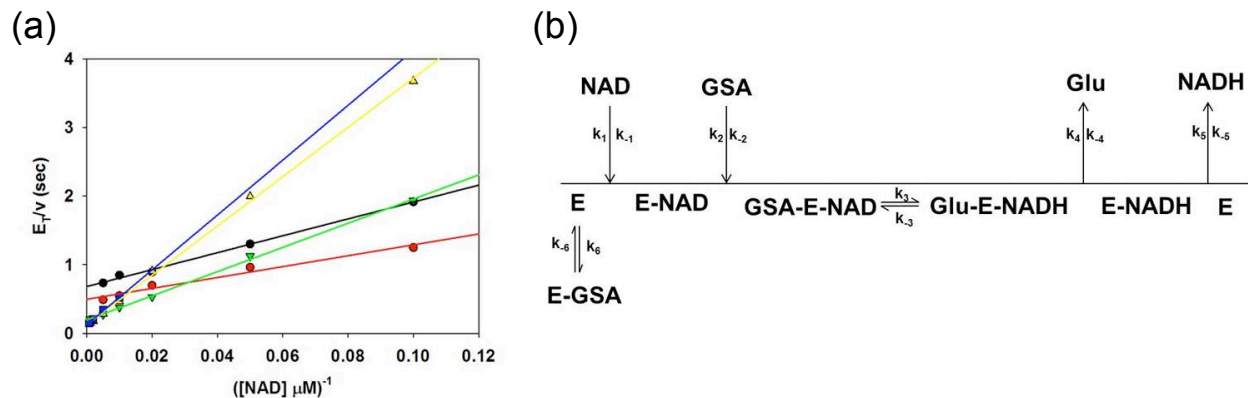


**Figure S5.** (a) Lineweaver-Burk analysis of initial velocity data for HsP5CDH collected with  $\text{NAD}^+$  concentrations in the range 10 - 1500  $\mu\text{M}$  in different fixed concentrations of a 50/50 mixture of DL-P5C with L-P5C concentrations as follows: 10 (black), 15 (red), 50 (green), 150 (yellow), 500  $\mu\text{M}$  (blue). Solid lines are the best-fit line to the individual data sets with the corresponding colored data points. (b) Kinetic scheme suggested by previously published data<sup>2</sup> but with an additional step for substrate inhibition as observed in panel A at higher P5C concentrations (150 and 500  $\mu\text{M}$ ). The original kinetic mechanism established for HsP5CDH was a Theorell-Chance mechanism, which is a limiting case of the scheme shown above where  $k_3$  and  $k_4$  are much faster than  $k_5$ .



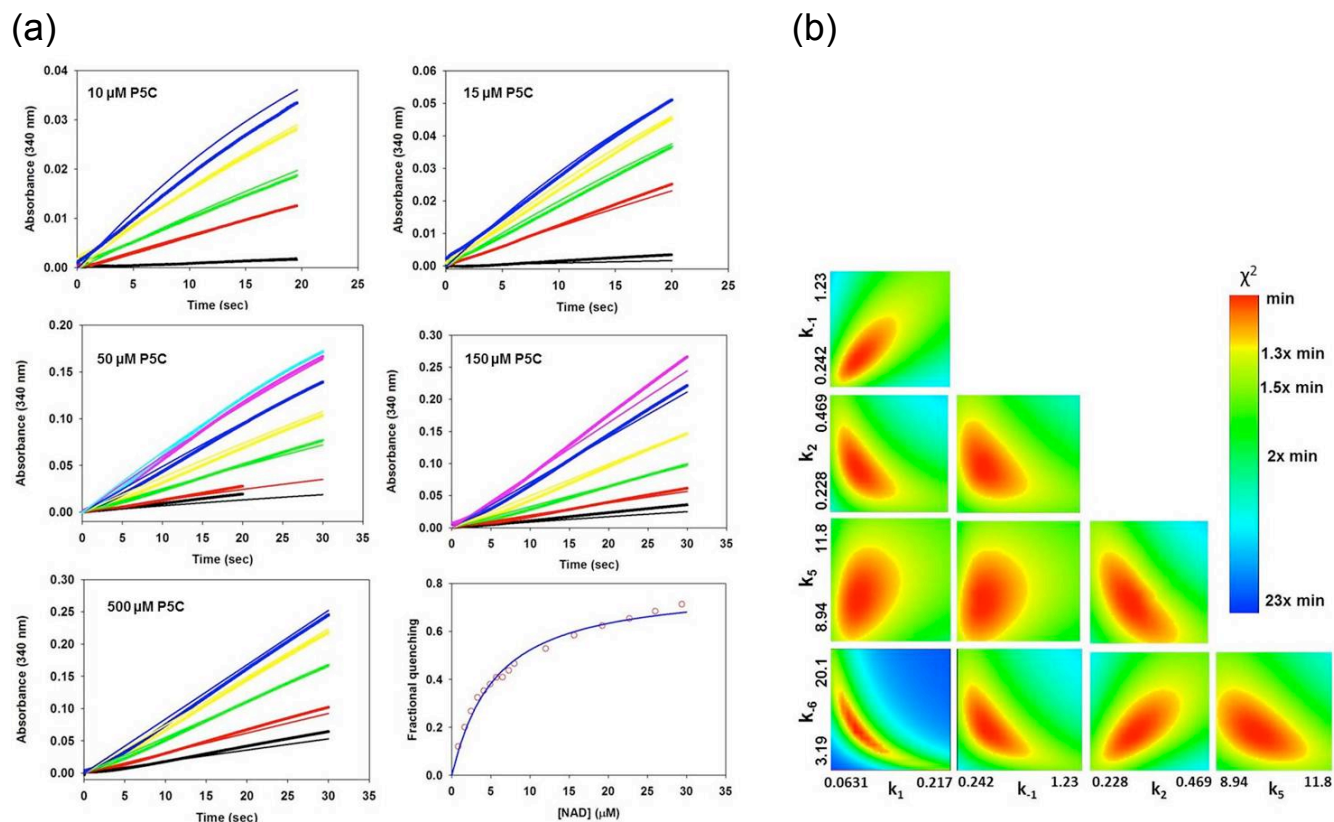


**Figure S6.** (a) Initial velocity progress curves for HsP5CDH at various NAD<sup>+</sup> concentrations (1-1500 μM) and different fixed L-P5C concentrations followed at 340 nm. Data were globally fitted to the simulated mechanism shown in Supplemental Figure 6B using KinTek Global Kinetic Explorer.<sup>3</sup> The bottom right graph shows a titration of HsP5CDH with NAD<sup>+</sup> monitored by tryptophan fluorescence quenching, which was also included in the global fitting analysis to help constrain  $k_1$  and  $k_{-1}$ . The rate constants for the chemical step ( $k_3$ ) and glutamate dissociation step ( $k_4$ ) were held fixed at values well above the NADH dissociation step ( $k_5$ ) in accordance with the Theorell-Chance mechanism.<sup>1</sup> (b) FitSpace<sup>4</sup> contour plots of the global fitting showing how variation in the fitted parameters affects the  $\chi^2$  value.

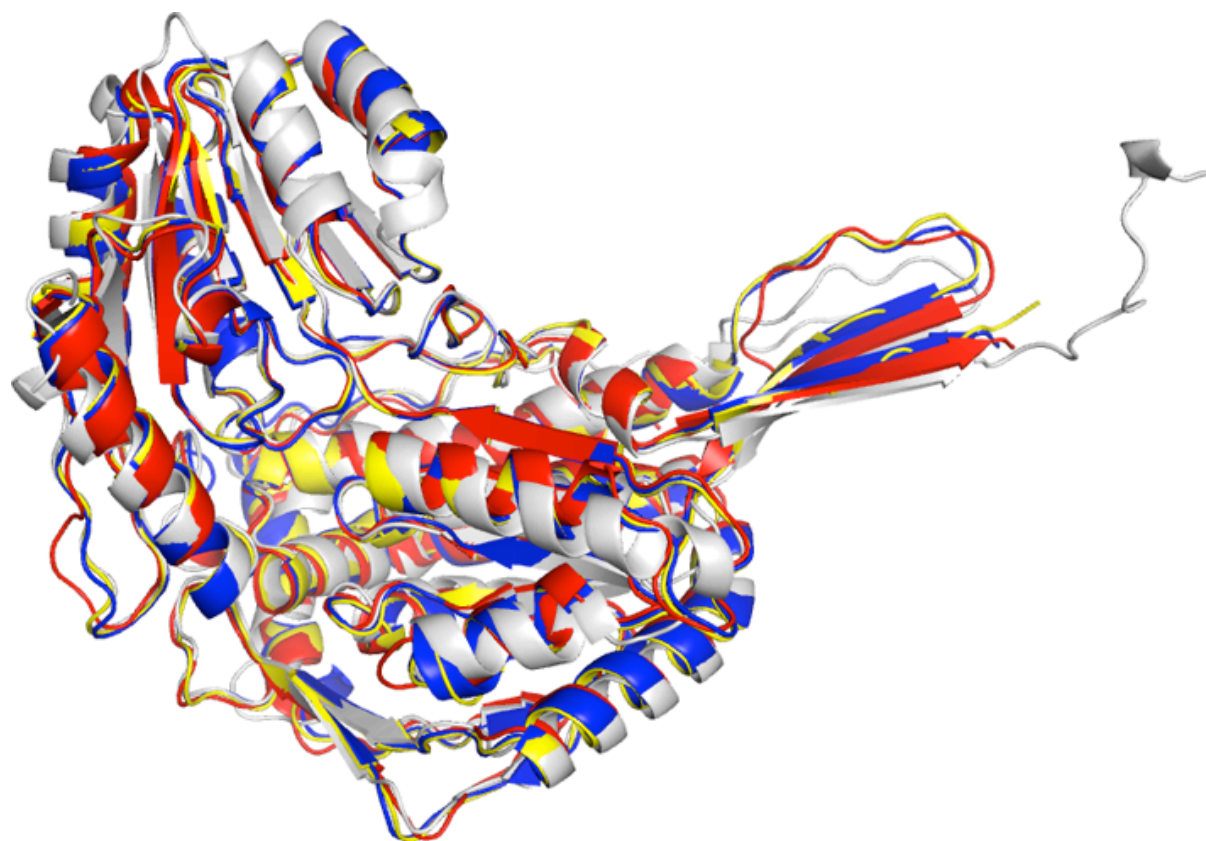


**Figure S7.** Superposition of HsP5CDH with bacterial P5CDHs from *Thermus thermophilus* (red, PDB code 2EIW), *Bacillus licheniformis* (blue, PDB code 3RJL), and *Bacillus halodurans* (yellow, PDB code 3QAN).

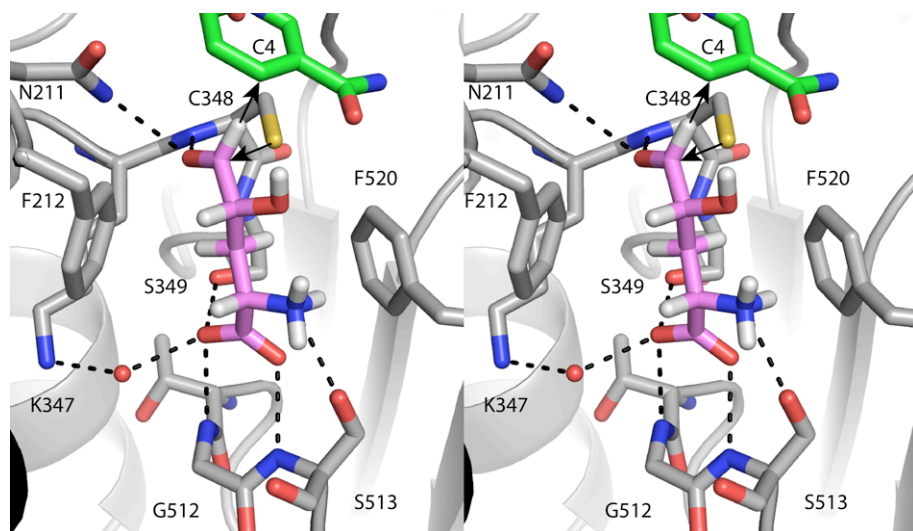


**Figure S8.** A model of OH-GSA bound to MmP5CDH (stereographic view). OH-GSA is shown in pink.  $\text{NAD}^+$  is colored green. The arrows depict the directions of nucleophilic attack by Cys348 and hydride transfer to  $\text{NAD}^+$ .

## Supplementary References

1. Cook, P. F. & Cleland, W. W. (2007). *Enzyme kinetics and mechanism*, Garland Science, New York.
2. Forte-McRobbie, C. & Pietruszko, R. (1989). Human glutamic-gamma-semialdehyde dehydrogenase. Kinetic mechanism. *Biochem. J.* **261**, 935-43.
3. Johnson, K. A., Simpson, Z. B. & Blom, T. (2009). Global kinetic explorer: a new computer program for dynamic simulation and fitting of kinetic data. *Anal. Biochem.* **387**, 20-9.
4. Johnson, K. A., Simpson, Z. B. & Blom, T. (2009). FitSpace explorer: an algorithm to evaluate multidimensional parameter space in fitting kinetic data. *Anal. Biochem.* **387**, 30-41.